

PL-TR-95-2079

---

## RADAR STUDIES OF AVIATION HAZARDS

F. Ian Harris  
David J. Smalley  
Shu - Lin Tung

Hughes STX Corporation  
109 Massachusetts Avenue  
Lexington, MA 02173

31 May, 1995

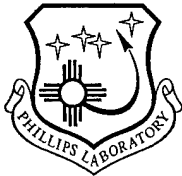
Scientific Report No. 2



---

APPROVED FOR PUBLIC RELEASE; DISTRIBUTION UNLIMITED.

---



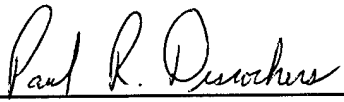
**PHILLIPS LABORATORY**  
Directorate of Geophysics  
AIR FORCE MATERIEL COMMAND  
HANSCOM AIR FORCE BASE, MA 01731-3010


---

19950807 047

DTIC QUALITY INSPECTED 5

"This technical report has been reviewed and is approved for publication."

  
\_\_\_\_\_  
PAUL R. DESROCHERS  
Contract Manager

  
\_\_\_\_\_  
DONALD A. CHISHOLM  
Chief, Satellite Analysis and Weather  
Prediction Branch  
Atmospheric Sciences Division

  
\_\_\_\_\_  
ROBERT A. McCLATCHEY, Director  
Atmospheric Sciences Division

This report has been reviewed by the ESC Public Affairs Office (PA) and is releasable to the National Technical Information Service (NTIS).

Qualified requestors may obtain additional copies from the Defense Technical Information Center (DTIC). All others should apply to the National Technical Information Service (NTIS).

If your address has changed, or if you wish to be removed from the mailing list, or if the addressee is no longer employed by your organization, please notify PL/IM, 29 Randolph Road, Hanscom AFB, MA 01731-3010. This will assist us in maintaining a current mailing list.

Do not return copies of this report unless contractual obligations or notices on a specific document requires that it be returned.

REPORT DOCUMENTATION PAGE			Form Approved OMB No. 0704-0188	
Public reporting burden for this collection of information is estimated to average 1 hour per response, including the time for reviewing instructions, searching existing data sources, gathering and maintaining the data needed, and completing and reviewing the collection of information. Send comments regarding this burden estimate or any other aspect of this collection of information, including suggestions for reducing this burden, to Washington Headquarters Services, Directorate for Information Operations and Reports, 1215 Jefferson Davis Highway, Suite 1204, Arlington, VA 22202-4302, and to the Office of Management and Budget, Paperwork Reduction Project (0704-0188), Washington, DC 20503.				
1. AGENCY USE ONLY (Leave blank)	2. REPORT DATE 31 May 1995	3. REPORT TYPE AND DATES COVERED Scientific Report No. 2		
4. TITLE AND SUBTITLE  RADAR STUDIES OF AVIATION HAZARDS			5. FUNDING NUMBERS  F19628-93-C-0054 PE63707F PR2781 TAGT WUMA	
6. AUTHOR(S) F. Ian Harris, David J. Smalley and Shu-Lin Tung				
7. PERFORMING ORGANIZATION NAME(S) AND ADDRESS(ES)  Hughes STX Corporation 109 Massachusetts Avenue Lexington, MA 02173			8. PERFORMING ORGANIZATION REPORT NUMBER  Hughes STX Scientific Report #2	
9. SPONSORING / MONITORING AGENCY NAME(S) AND ADDRESS(ES) Phillips Laboratory 29 Randolph Road Hanscom AFB, MA 01731-3010  Contract Manager: Paul R. Desrochers/GPAB			10. SPONSORING / MONITORING AGENCY REPORT NUMBER  PL-TR-95-2079	
11. SUPPLEMENTARY NOTES				
12a. DISTRIBUTION / AVAILABILITY STATEMENT Approved for public release; distribution unlimited			12b. DISTRIBUTION CODE	
13. ABSTRACT (Maximum 200 words) Hughes STX is developing algorithms/techniques that are targeted for use with the WSR-88D weather radars. Phenomena being addressed are precursors to severe weather, precursors to lightning, and the monitoring of potentially hazardous weather associated with baroclinic front situations. Progress made during the past year in each of the algorithms is outlined.				
14. SUBJECT TERMS  Doppler weather radar, automated techniques, storm structure, severe storms, lightning precursors, front detection, gradient computation			15. NUMBER OF PAGES 28	16. PRICE CODE
17. SECURITY CLASSIFICATION OF REPORT Unclassified	18. SECURITY CLASSIFICATION OF THIS PAGE Unclassified	19. SECURITY CLASSIFICATION OF ABSTRACT Unclassified	20. LIMITATION OF ABSTRACT Unlimited	

# TABLE OF CONTENTS

<b>1. INTRODUCTION</b>	<b>1</b>
<b>2. SEVERE STORM STRUCTURE</b>	<b>1</b>
2.1 INTRODUCTION	1
2.2 ALGORITHM DEVELOPMENT	2
2.3 PURCELL, OK SUPERCELL CASE	7
2.4 FUTURE RESEARCH	11
<b>3. LIGHTNING PREDICTION IN AIR MASS THUNDERSTORMS</b>	<b>11</b>
<b>4. FRONTAL STRUCTURE</b>	<b>13</b>
4.1 INTRODUCTION	13
4.2 THE FRONT	13
4.3 FRONT DETECTION	15
4.3.1 Gradient Algorithm in Polar Coordinates	16
4.3.2 Front Extraction Procedure	18
4.4 FRONTAL STRUCTURE	18
4.4.1 Radial Velocity	18
4.4.2 Reflectivity	19
4.4.3 Gradients	20
4.5 SUMMARY	21
<b>5. DEVIATIONS FROM RESEARCH PLAN</b>	<b>22</b>
<b>6. PLANS FOR NEXT CONTRACT YEAR</b>	<b>22</b>
<b>7. REFERENCES</b>	<b>22</b>

Accession For	
MHS GRAS	<input checked="" type="checkbox"/>
DTIC TAB	<input type="checkbox"/>
Unannounced	<input type="checkbox"/>
Justification	
By _____	
Distribution/Avail _____	
Availability Codes	
Dist	Avail and/or Special
A-1	

## LIST OF FIGURES

1. The identified BWER at 2323 UTC superimposed on the contoured reflectivity field. ....	8
2. The identified WER at 2322 UTC superimposed on the contoured reflectivity field.....	9
3. The three-dimensional lateral extent of the identified BWER/WER at 2323 UTC.....	10
4. Radial velocity field at 0.5° elevation. ....	14
5. Three-dimensional depiction of the 35dBZ reflectivity isosurface superimposed upon the reflectivity data for the 0.5° elevation scan.....	15
6. Gradient magnitudes for the velocities in Figure 4. ....	16
7. Frontal position as detected at 0.5° elevation and RHI displays of radial velocity at 226°, 260°, and 290° azimuth. ....	19
8. RHI displays of reflectivity as in Figure 7.....	20
9. As in Figure 8 but for velocity gradients. ....	21

## LIST OF TABLES

1. Weight Factors Used for BWER Identification .....	7
2. Output Parameters from Volumetric Statistical Module.....	12

## **1. INTRODUCTION**

This report presents a summary of the research conducted during the past year and a brief presentation of plans for the upcoming year. The goal is for Hughes STX to develop and test algorithms/techniques that will be candidates for inclusion in the NEXRAD algorithm inventory. Phenomena of particular interest to the Air Force are being addressed: precursors to severe weather (tornadoes, hail, severe wind events), precursors to lightning development, and monitoring of potentially hazardous weather and wind associated with baroclinic front situations. Efforts in each of these three areas will be described in turn. For a discussion of the overall goals of this task and a summary of activities for the first year of the contract, please see the first annual report for this contract (Harris et al., 1994).

During this year, there were two distinct phases to all three tasks. The first was a rather slow and ponderous development of algorithms and code on the personal computers and the VAX 3100. Midway through the research year, the new Hewlett-Packard workstations were delivered and the process of learning the UNIX operating system and converting code to these systems began. In addition, a sophisticated visualization software package (Application Visualization Software - AVS) was delivered. Once familiarization of the new hardware and software reached a "working level," progress in all tasks was very much accelerated. The speed and efficiency of the new hardware and the tremendously improved analysis capability of the new software have greatly enhanced productivity.

## **2. SEVERE STORM STRUCTURE**

### **2.1 INTRODUCTION**

Tornadoes, hail, flash floods, and other severe weather have long been associated with thunderstorms. The most infrequent and severe thunderstorms, known as supercells, account for a disproportionately large percentage of all thunderstorm-related mayhem. These supercells are distinguished from ordinary

thunderstorms by the presence of an exceptionally persistent, powerful, and organized updraft and by a distinctive radar reflectivity structure. Browning and Donaldson (1963) compared a western United States supercell with one in Great Britain. Each exhibited an echo-free vault beneath a high reflectivity core that they attributed to the updraft. Chisholm (1973) named similar vaults in Alberta supercells as Weak Echo Regions (WERs) or, if completely surrounded by high reflectivity, Bounded Weak Echo Regions (BWERs). The basic supercell structure also consists of a reflectivity core aloft and mid-level echo overhang.

It is not possible to directly measure the updraft with a single scanning Doppler radar. However, it is possible to infer updraft characteristics, such as strength, spatial extent, and persistence, by monitoring reflectivity features within the storm. The most distinct structure that is usually associated with very strong updrafts is the BWER. It appears because precipitation particles are swept upwards within the main updraft before there can be appreciable growth. These particles are then carried away from the updraft region by the divergent flow aloft and allowed to fall in a ring around the updraft. Because the BWER is a product of the updraft, monitoring characteristics of the BWER should provide insight to updraft strength, size, and persistence. The current suite of NEXRAD algorithms does not include any algorithms that identify or quantify BWER or WER features. The closest product is the volume WER described by Klazura and Imy (1993) which consists of a display of eight stacked slices of reflectivity. To provide this monitoring capability, Hughes STX is developing a real-time algorithm to quantify severe storm structures in two- and three-dimensions and to correlate trends in these structures to the occurrence and type of severe weather. Such an algorithm is intended to complement the mesocyclone algorithm.

## ***2.2 ALGORITHM DEVELOPMENT***

The BWER is visually identified in radar data collected at a constant elevation angle as a ring or ridge of high reflectivity surrounding a distinct minimum. Outside

the ring, reflectivity decreases. Thus, the primary image characteristics of a BWER are:

- a high reflectivity ridge,
- a transition of high-low-high reflectivity across the feature, and
- reflectivity gradients.

An algorithm to identify and quantify these characteristics of the BWER has been developed and, to some degree, extended to identify and quantify WERs. Both model and control cases were used to develop BWER identification concepts applicable to the reflectivity field. A simple model was constructed where the reflectivity structure includes a minimum in the center with a linear increase in reflectivity in all directions to a maximum at a specified radius. Beyond this maximum, the reflectivity decreases linearly with distance. The resultant pattern resembles a circular ring. The control case is the 5<sup>0</sup> elevation scan at 2303 UTC from the Piedmont, OK storm of April 30, 1978. This storm was close to the radar (< 55 km range) and produced a F4 tornado. The BWER within this storm was relatively short-lived (5 minutes) and was best defined in the selected scan at 2303 UTC. Model data were used to develop the concepts and to test the software. The resultant concepts were then applied to the control data to perform initial assessments and technique refinement.

Identification of the BWER uses pattern recognition techniques similar to those used by the MIT/Machine Intelligent Gust Front Algorithm (Delanoy and Troxel, 1993). Independent analyses of the original data are performed to generate various derived fields. The fields themselves are combined through weighting functions to identify the WER/BWER. Because each analysis is independent, this methodology is essentially a parallel analysis scheme and differs from conventional processing that generates products in a serial manner. Data are processed in spherical space to reduce the computational load. Coordinates are introduced only after the structural feature is identified.

The primary processes that have been implemented to derive field characteristics are:



- identification of regions of highest reflectivity associated with the core region of the storm,
- isolation of local maxima and minima (extrema) in the data field,
- computation of gradient magnitude and direction with orthogonal Sobel operators,
- identification of a high-low-high (HLH) reflectivity magnitude pattern either along or across radials.

The concept of pattern vectors has been used in the computation of the local extrema and the HLH patterns. Pattern vectors join the first and last data values along or across radials where all the gate-to-gate changes in field values (local derivatives) have the same sign. The direction of the vector is determined by the sign of the changes while the length is determined by the number of data points that have been connected.

Weights are applied to the results from these independent analyses and combined with weighted secondary information (such as pattern vector length) to yield the BWER ridge outline. This technique is also used for the identification of WERs that appear as broad notches in the reflectivity image. However, thunderstorms are noted for their complex structures, including relatively benign reflectivity notches. As a result, considerable care must be taken in the identification of WERs to minimize false detections. Multilevel position correlation may be needed to isolate true WERs from the benign notches.

The first three of these procedures are discussed extensively in Harris *et al.* (1994). They showed that a substantial percentage of cells that comprise the control BWER ridge was identified. However, other features were also identified, thereby impeding isolation of the BWER ridge.

A significant enhancement to the identification techniques for the BWER ridge is the addition of the HLH pattern analysis. This analysis uses binary coding to identify those cells with reflectivity magnitudes in the lowest 20% of the current sample. Binary coding is simply the assigning of the number one to data values that pass a specific test and zero to those that do not. In this case, all points that have

reflectivity values in the lowest 20% are assigned a value of one and all others are 0. Fields from this analysis are then combined with the high reflectivity cell analysis to identify the HLH patterns. This information is then one of the weighted analyses combined to yield the BWER ridge signature.

This HLH enhancement resulted in the elimination of spurious features and the successful identification of the control BWER ridge. However, this technique requires refinement. In the volume following that of the control BWER, a BWER ridge was visually apparent in the data but the algorithm could not successfully identify it because the HLH input was zero. The BWER had apparently begun to fill, thereby reducing the contrast in reflectivity values between the ridge and the hole. Thus, it would appear that the algorithm is susceptible to overlooking BWERs whose ridges envelop regions with only slightly weaker reflectivity. Those situations might be expected to occur during the initial and decaying stages of a BWER or with weakly developed BWERs. Of course, analysis of many storms will be required to better appreciate the life cycle of the structure of BWERs.

The data processing flow of the algorithm is as follows:

- The data domain is areally cropped to focus on the core region of the storm. This process selects the range and azimuth bounds that include all values of reflectivity within the storm volume that are above a specified threshold.
- Noisy data are eliminated. Data values that fall outside 2.5 standard deviations of a 25 cell neighborhood mean are identified and replaced with the mean of an 8-neighbor mask centered on the target cell.
- The data volume is cropped still further to reduce processing load and to eliminate the potential for false alarms. This processing step is defined in detail in Harris et al. (1994).
- Reflectivity pattern vectors along and across radials are constructed for the core region. Locations of extrema and lengths of associated pattern vector pairs are determined.

- Gradient magnitudes and directions are computed using orthogonal Sobel operators. Harris *et al.* (1994) describe in detail the generation of these fields.
- Reflectivity values are sorted based on reflectivity value. The top 20% values and the bottom 20% values are converted to separate binary fields. These fields are then used to locate the high reflectivity regions and to derive the HLH patterns.
- Results from the above described analyses are combined through weights to yield the outline of the BWER/WER features.

Most of the algorithm development was performed in DEC VAX and Microsoft DOS environments. During the last quarter of this contract year, resultant software has been converted to operate in an HPUX environment on Hewlett Packard 715/100 Unix workstations and with the Advanced Visualization Software (AVS). The original algorithm was recoded as needed for proper implementation within the new system environment. The most significant advancement came with the conversion to modules for use with AVS. This enabled the easy and timely manipulation of variables and three-dimensional visualization of the results and allowed the more efficient assessment of algorithm performance. Many of the hard-coded variables in the original algorithm are now controlled interactively with widgets in AVS. This interactive capability permitted sensitivity assessments of the various parameters. Widgets have also been employed to control the weights used to combine the analyses into an identification of a BWER or WER. Now, any or all of the weights can be changed and the resultant identification instantly monitored.

With the conversion to the new workstation environment, the newly designed algorithm was applied to WSR-88D data collected from a supercell storm near Purcell, OK. This has resulted in some changes to the weights that were derived from the control BWER. Table 1 lists the weight name, the weight for the control BWER case, and the new adjusted weight. Further discussion of the analysis of this storm is found in the next section.

For each volume of each storm, a contiguous stack of roughly 30 km x 30 km planes (one from each elevation scan) is identified as the core reflectivity region of

Table 1. Weight Factors Used for BWER Identification

<i>WEIGHT NAME</i>	<i>OLD WEIGHT</i>	<i>NEW ADJUSTED WEIGHT</i>
top 20% high reflectivity	1	1
extrema location	1	0
HLH cell yes/no	1	1
gradient magnitude	0.25	0
gradient direction	0.25	0.25
extrema pattern vector length	0	0

the storm. This core region is processed to isolate BWER (and WER) ridges. These ridge outlines are then used to determine area and volume characteristics of the individual (two dimensional) and composite (three dimensional) features. Additional volume and area characterizations will be explored.

### **2.3 PURCELL, OK SUPERCELL CASE**

On September 2, 1992, a supercell caused severe weather southwest of Purcell, OK. There were reports of large hail and, for about one half hour, a tornado (F2) with an 8 - 9 mile path (Branick, 1992). The WSR-88D in Norman, OK that supports the Operational Support Facility for the NEXRAD program was the closest system to the storm. Recording of Archive II data with this system began three minutes after initial tornado touchdown. The first six volumes (one per six minutes) that correspond to the lifetime of the tornado were processed by the algorithm.

The storm at this time exhibits most of the trademark severe weather signatures: BWER, WER, hook echo, TVS, and mesocyclone. In the first volume, the algorithm

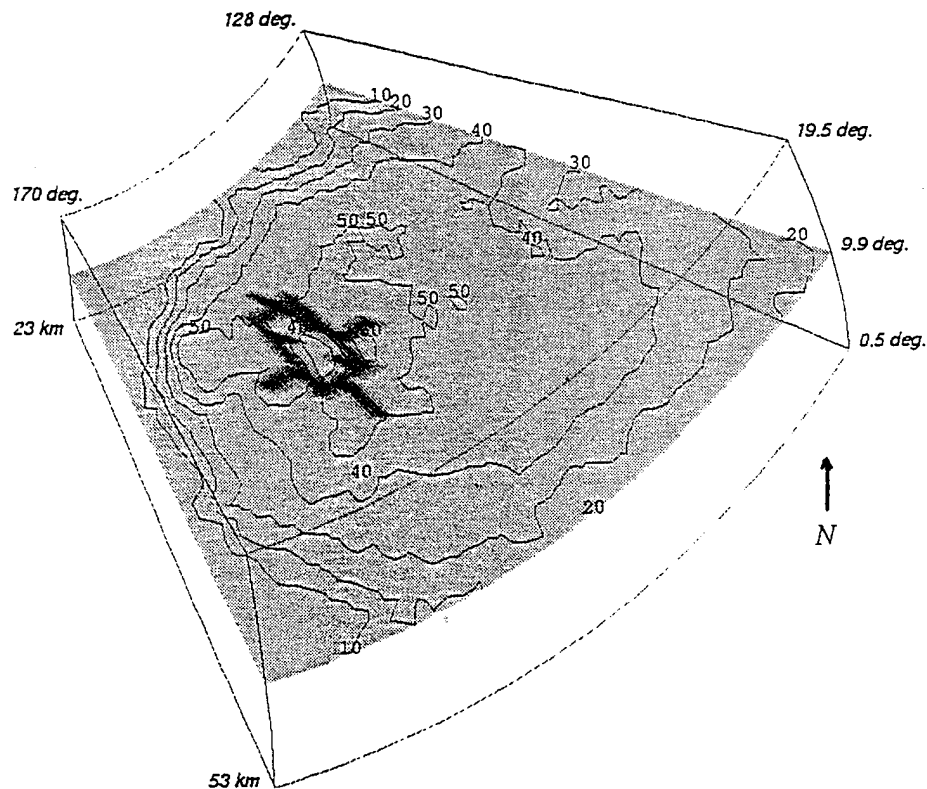


Figure 1: The identified BWER (dark outline) at 2323 UTC superimposed on the contoured reflectivity (dBZ) field,

successfully identifies the BWER in the scan at  $9.9^{\circ}$  elevation angle and the WER in the scan immediately below it at  $6.0^{\circ}$ . These features are well defined at this stage. Figure 1 shows the reflectivity core region for the BWER level for the first volume (2323 UTC) with the identified ridge superimposed. The BWER is centered about 35.2 km from the radar at an azimuth of  $154^{\circ}$  with an approximate altitude of 6.2 km AGL. It covers an area about  $26.6 \text{ km}^2$ . Observe that the identified outline encompasses the 40 dBZ contour within the broad 50 - 60 dBZ region.

Figure 2 depicts the WER at the next available level below the BWER level of Figure 1. The WER is centered about 36.1 km from the radar at  $156^{\circ}$  with an altitude of 3.9 km and covers an area about  $32.9 \text{ km}^2$ . Notice that the outline encompasses the WER in which the reflectivity values drop below 20 dBZ. At lower elevation angles, the WER structure is not as well defined and only partial identification is achieved.

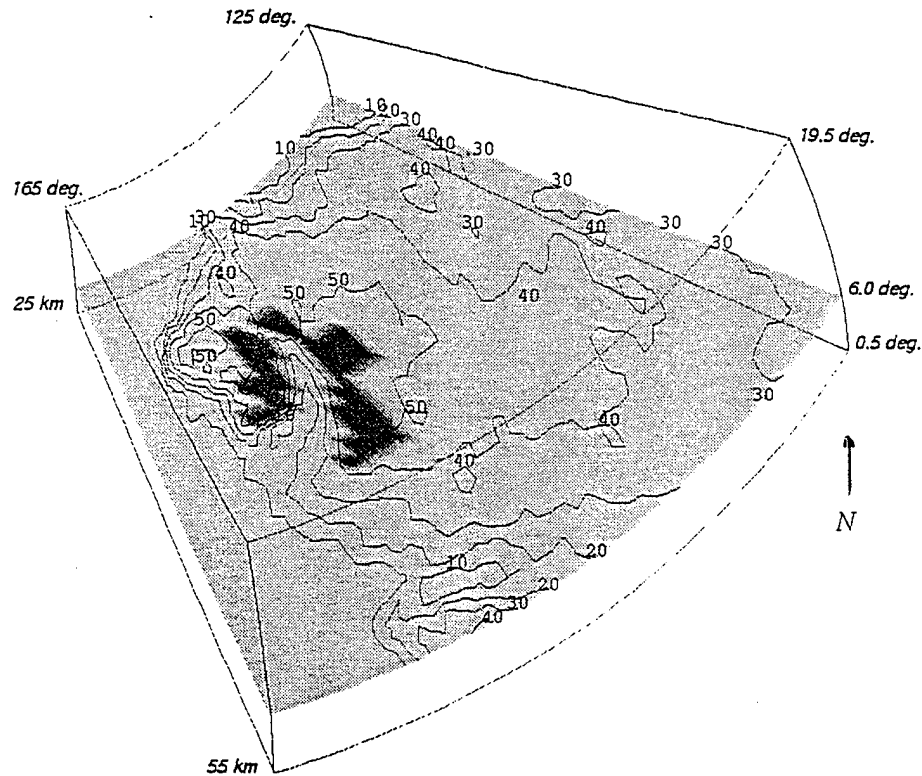


Figure 2: The identified WER (dark outline) at 2322 UTC superimposed on the contoured reflectivity (dBZ) field. The plane shown is for the  $6.0^\circ$  elevation scan. The radar is to the northwest. Refer to the text for further details.

When the results of the algorithm from these two elevation levels are combined along with the knowledge that the feature is capped by the next higher plane, an estimate of feature volume is possible. Figure 3 shows the three-dimensional surface of the lateral extent of the BWER/WER ridge for the first volume. This depiction suggests that the updraft enters the supercell from the southeast at low levels. At mid-levels, it becomes completely bounded as it rises through the storm (out of the page at an angle toward the top of the page). If the next plane were included, the surface of this feature would come together from all sides to create a closed top. Once the three-dimensional structure of the BWER/WER has been determined, volumetric statistics can be estimated. For example, the volume of the BWER/WER is about  $128.4 \text{ km}^3$  and its reflectivity weighted centroid is about 36.1 km from the radar at  $156^\circ$  with an altitude of 4.0 km. The next step will be to look at statistics such as these as a function of time to determine trends and to relate the trends to tornado activity. It is to be noted that, for this example, the large angular

separation of the elevation scans leads to coarse estimates of the volume. Use of the severe weather scan strategy, instead of the precipitation mode that was used, would have resulted in a better scan resolution than that shown here.

For the second volume scan (beginning at 2324 UTC), the algorithm detects the BWER/WER pair previously identified. Again, structural complications at lower levels precluded successful isolation of the WER below. The BWER and WER were both larger (not shown) at this time. The physical characteristics expanded about 67% from the previous scan. Analysis of the third volume scan revealed the BWER had filled but the WER was still identified. Subsequent filling continued to lower levels in the succeeding volumes as the tornado continued.

At its current level of development, the algorithm successfully identifies the well-defined BWERs and WERs in the Purcell storm. The algorithm did have difficulty with the WER at lower levels because of significantly greater complexity to the

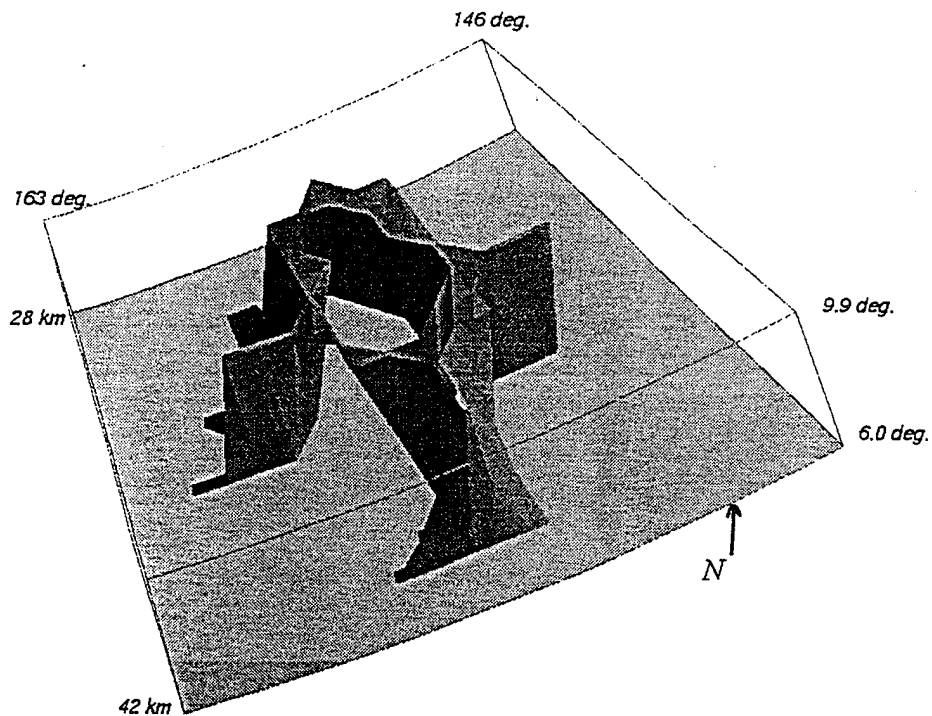


Figure 3: The three-dimensional lateral extent of the identified BWER/WER at 2323 UTC.

reflectivity structure. Some area and volume quantification was also included to illustrate the capabilities to be included in the algorithm.

## **2.4 FUTURE RESEARCH**

The current state of development of an algorithm to detect WERs and BWERs and quantify these structures is described. A case study of the 1992 Purcell, OK supercell is discussed with volumetric and areal quantities provided. Unfortunately, data were not available prior to the tornado. The intent of the quantification information is to monitor the development of BWERs and WERs prior to the onset of severe weather to provide an additional tool for the forecaster. For the future, the development of many more supercells will be examined. It is expected that, with a large data set of storms, generalizations will follow to maximize the potential of identifying structures in storms not as well defined as with the Purcell case. Another aspect being considered is the use of multilevel correlation for better feature recognition particularly for WERs. The early results are encouraging and we anticipate enhanced performance as experience is gained.

## **3. LIGHTNING PREDICTION IN AIR MASS THUNDERSTORMS**

The goal for this task is to develop parameters that will give indicators of the onset of lightning activity. There have been many studies relating the evolution of reflectivity structure to lightning but no one has attempted to adapt these studies to a real time application. In this study, we are attempting to perform this transition. One of the biggest problems with this task has been the availability of appropriate data. Data have been collected by specialized groups but these data were not readily available. With their procurement of the new state of the art workstations, the government has allowed us the potential of assessing the vast data sets currently being amassed within the WSR-88D program.



Table 2. Output Parameters from Volumetric Statistical Module

Domain	Parameter
Plane	area within thresholds
	field-value weighted areal centroid
	area-weighted mean of field values
Storm	volume within thresholds
	field-value weighted volumetric centroid
	Volume-weighted mean of field values.

Precipitation distributions within convective storms have been correlated with the onset of precipitation. Some of the parameters that have been examined by others include the top of the radar echo, rate of growth of echo top, the maximum reflectivity above  $-10^{\circ}$  C, height of maximum reflectivity within the storm. These are all parameters that can be monitored automatically in real time. With this in mind, software was written to compute areal and volumetric statistics on any three-dimensional scalar field. This software thresholds the data such that all values upon which the statistics will be based are between specified extremes. It then computes representative areas and volumes for each data value (Table 2). These statistics are then to be monitored with time and assessed as to potential for lightning prediction. Other applications for these parameters are to assess the general development of the storm. They will give an assessment of the rate of precipitation development, the stage of storm development, the amount of precipitation storage, etc. If the storm mass is increasing with time and the bulk of the precipitation growth is aloft, then this is important information with regard to future precipitation fallout, as a minimum. The amount of precipitation stored aloft can also be a function of the strength of the updraft and therefore the potential severity of the weather that will or is being produced. If the precipitation is observed to be descending with time, then this is probably an indicator of the storm entering the decay stage. It can also be an indicator of the onset of severe weather since many severe weather events are

observed to be correlated with the collapse of the updraft and associated precipitation structure aloft.

In the coming year the structure module described above will be applied to reflectivity factor and to gradients of radial velocity to assess its potential as a lightning precursor tool.

## **4. FRONTAL STRUCTURE**

### **4.1 INTRODUCTION**

Fronts are regions of transition in the temperature and wind fields and their intensity is usually assessed in terms of the magnitudes of the temperature changes and associated wind velocities. Cold fronts, especially, are noted for sharp changes in both temperature and winds. In addition, associated localized intense convection will enhance these fields and may cause severe weather. Fronts always occur in pressure troughs and will always have localized vorticity and convergence maxima. Therefore, monitoring vorticity and divergence in real time could provide useful diagnostic and prognostic information. Single Doppler radar cannot measure these fields individually. However, the radial velocity fields reflect a combination of these fields and can therefore be useful in the detection and monitoring of the fronts and associated phenomena.

In this report, we present the three - dimensional structure of a front as observed by the Phillips Laboratory Doppler radar located in Sudbury, MA. The analysis first employs pattern recognition techniques to manipulate the radar images. Then, two- and three-dimensional visualization techniques are used to gain a better understanding of the frontal structure.

### **4.2 THE FRONT**

The data used for the analysis were collected from a well-developed cold front episode by the PL Doppler radar at 1608 EST, 16 November 1989. This radar has a wavelength of 11.07 cm and a beam width of  $1.0^\circ$ . The data were collected at gate spacing of 0.15 km, azimuthal spacing of  $0.7^\circ$ , and a Nyquist velocity of 27.65 m/s.

Figure 4 is a gray-shade image view of the radial velocity field associated with this front. There is a distinct line running north-south to the west of the radar. This line delineates the strong southerly flow ahead of the front from the predominately westerly flow behind.

In Figure 5, the three-dimensional 35 dBZ isosurface is superimposed on the radial velocity field of Figure 4. This surface has the appearance of a line oriented parallel to and ahead of the low-level wind discontinuity. Observations of rainbands that are parallel to and either behind or straddling an active surface cold front are well-documented (e.g., Browning and Harrold, 1970, and Hobbs et al., 1978).

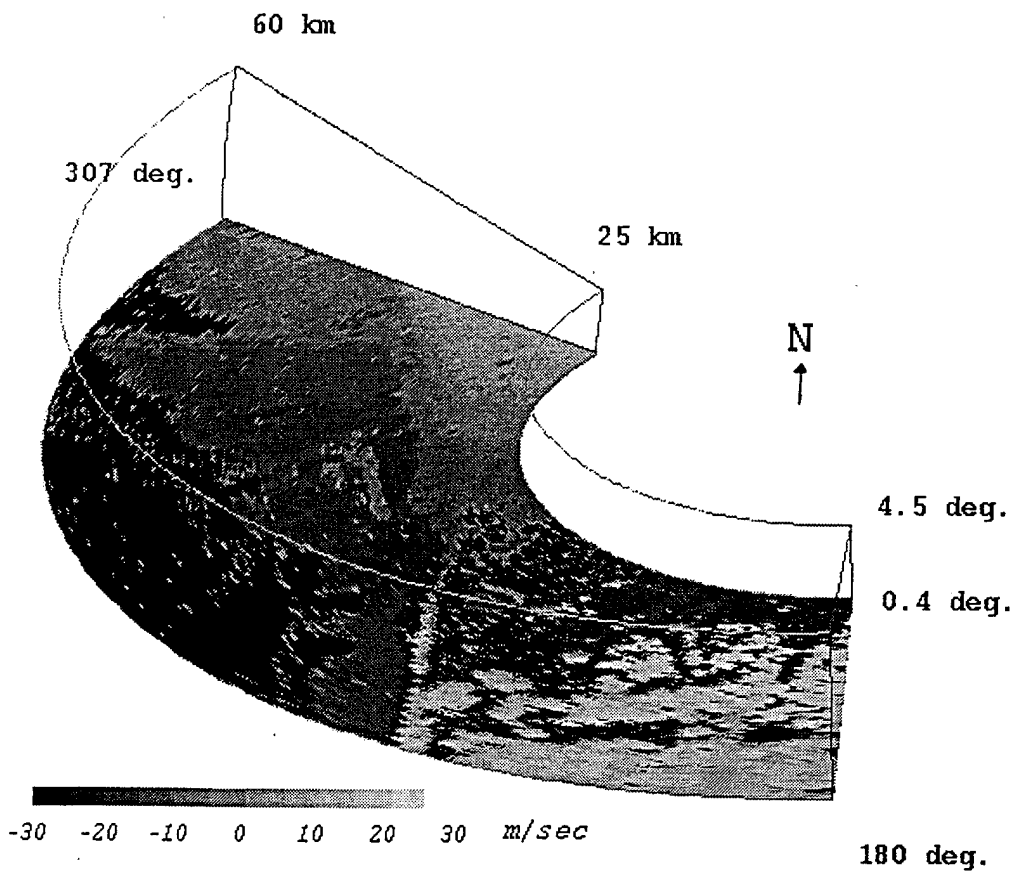


Figure 4. Radial Velocity field at  $0.5^\circ$  elevation. The lighter (darker) shades represent data towards (away) from the radar.

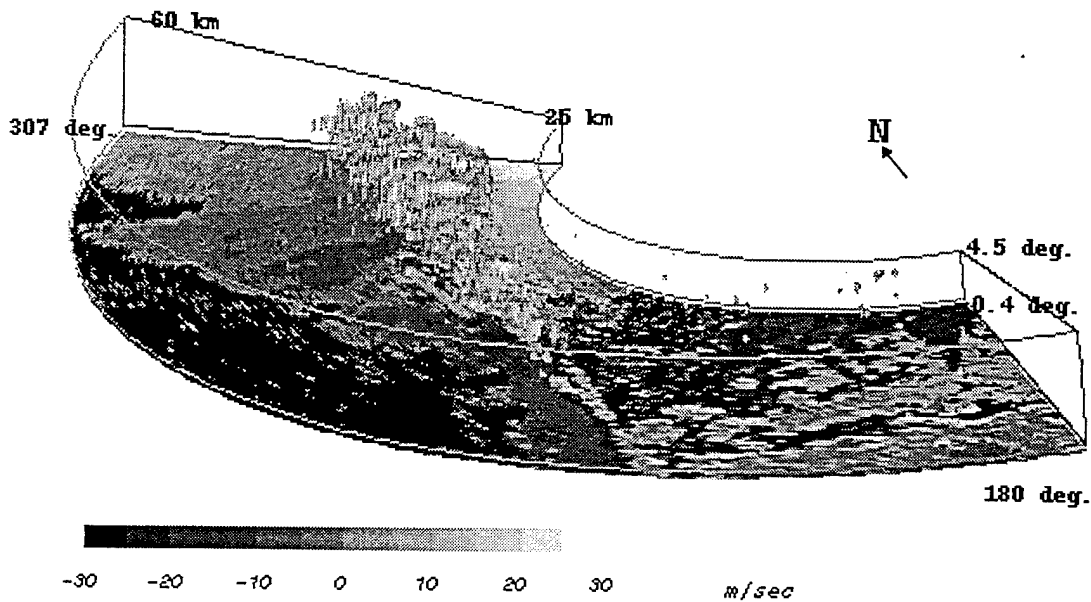


Figure 5 Three-dimensional depiction of the 35 dBZ reflectivity isosurface superimposed upon the reflectivity data for the 0.5° elevation scan.

### 4.3 FRONT DETECTION

A series of computer vision algorithms has been implemented to isolate fronts and to study their structure. For front isolation, a two-dimensional front extraction technique has been developed. This technique uses common visualization approaches based on the detection of edges of objects. Edges are typically associated with regions of sharp gradients in data fields. Fronts often have distinct convergence lines in the velocity field and lines of enhanced reflectivities (Wilson and Schreiber, 1986). In the reflectivity field, because the largest gradients tend to be on the boundaries of the echoes, edges based on gradients can usually define the perimeter of the radar echo. In radial velocity fields, large gradients tend to occur across the wind shift lines associated with fronts. In this case edge detection based on gradients should be very effective as a front detection tool.

Analysis is performed in the natural spherical coordinate reference frame in which the data were collected. First, two-dimensional analysis routines are applied to individual elevation scan planes. Then, results from these analyses are combined to produce a coherent depiction of the front. The techniques used for gradient computations and feature integrations are similar in principle to, but differ in detail from, those developed by Hamann (1991) and Delanoy and Troxel (1993).

#### 4.3.1 Gradient Algorithm in Polar Coordinates

A two-dimensional gradient algorithm in polar coordinates has been developed for Doppler radar data. The gradient for a scalar field in polar coordinate space ( $r$  - range,  $\theta$  - azimuth) can be expressed as

$$\nabla f(r,\theta) = \left( \frac{\partial f(r,\theta)}{\partial r}, \frac{\partial f(r,\theta)}{\partial \theta} \cdot \frac{\partial \theta}{\partial s} \right) \quad \text{where } \frac{\partial \theta}{\partial s} = \frac{1}{r}$$

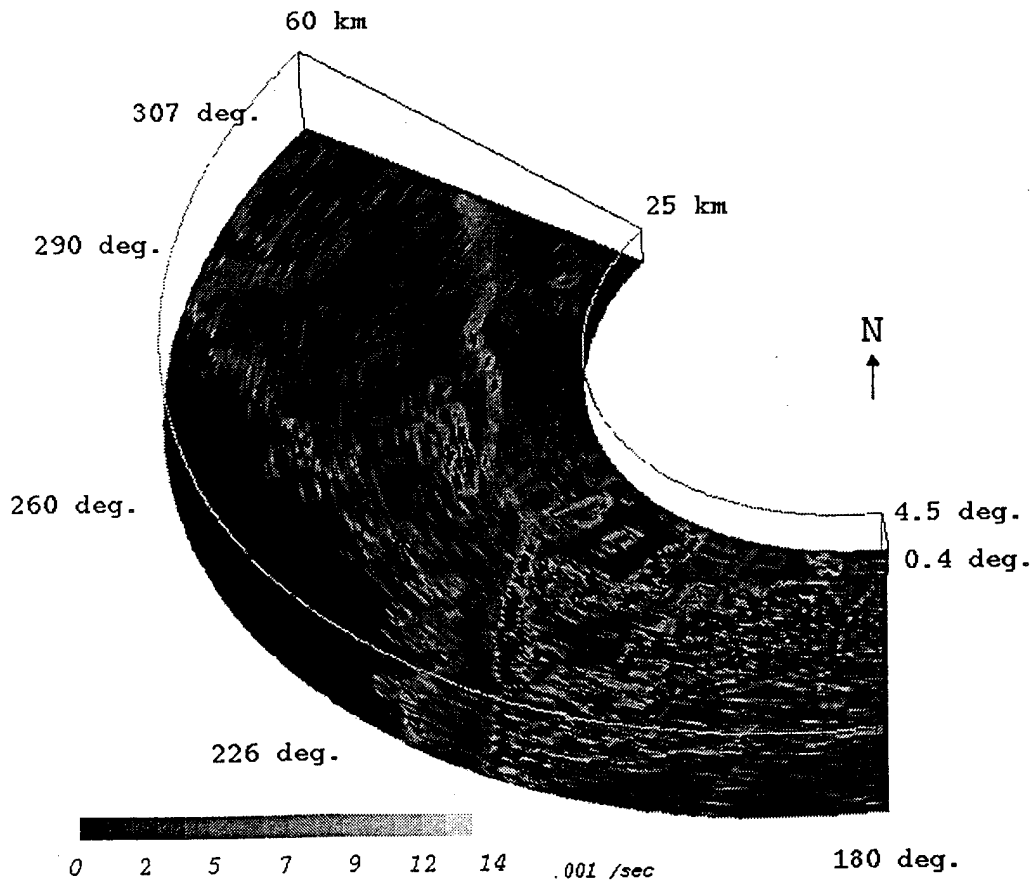


Figure 6. Gradient magnitudes for the velocities in Figure 4.

In these expressions,  $s$  is distance along an arc at range  $r$ . To compute these gradients, a pair of finite difference templates are applied. These templates yield the two components of the local gradient from which the magnitude ( $G$ ) and direction ( $\phi$ ) of the gradient vector are computed from the difference operators along the directions (1 and 2) as

$$G = (\Delta_1^2 + \Delta_2^2)^{1/2} \text{ and } \phi = \tan^{-1}(\Delta_2 / \Delta_1)$$

$$\text{where, } \Delta_1 \sim \frac{\partial f(r, \theta)}{\partial r} \text{ and } \Delta_2 \sim \frac{\partial f(r, \theta)}{\partial \theta} \cdot \frac{\partial \theta}{\partial s}$$

It should be noted that, prior to application of the gradient templates, it is necessary to ensure that all radial velocity data have been properly dealiased. Otherwise, artificially enhanced gradients will be produced. To mitigate the effects of folded data, a simple velocity unfolding technique based on pattern recognition is used. The data are quantified into four equal velocity intervals within the Nyquist velocity range, with each interval being assigned an index and sign. The sign corresponds to the sign of the measured velocity. A map of these indices clearly depicts regions where the data are inconsistent with the surroundings due to aliasing. The data in these regions are then dealiased.

The gradient algorithm generates an output field of vectors for each elevation plane. Vector directions are orthogonal to the local contour lines. Figure 6 shows the gradient vector magnitudes for the radial velocity field of Figure 4 with brightness proportional to vector magnitude. A distinct line of large magnitudes is observed to extend north-south. This line is coincident with the velocity discontinuity seen in Figure 4 and is parallel to the reflectivity line of Figure 5.

### **4.3.2 Front Extraction Procedure**

Next, edge extraction from the two-dimensional gradient fields is performed. Those regions with large gradient magnitudes and somewhat coherent vector directions are isolated in both the reflectivity and Doppler velocity fields. This sometimes results in multiple regions, some of which have no relationship to the front in question. To eliminate small, insignificant regions, image thresholding is applied. Then, the front is identified with the use of fuzzy logic to combine edges from the velocity and reflectivity fields and reflectivity magnitudes into a coherent frontal zone. Figure 7 depicts the resultant frontal feature in association with constructed RHIs of the radial velocity.

## **4.4 FRONTAL STRUCTURE**

### **4.4.1 Radial Velocity**

In Figure 7 the RHI plots of Doppler velocity data are at azimuths of  $226^\circ$ ,  $260^\circ$ , and  $290^\circ$  along with the surface position of the front as reference. The plane at  $290^\circ$  has a distinct velocity discontinuity at about 35 km range. This discontinuity is coincident with the surface frontal position and has distinct vertical continuity. There appears to be no significant slope to this front, at least up to the last observed height (about 2.5 km). In the next RHI (at  $260^\circ$ ) further south along the front, we see less vertical structure in the data. This RHI is oriented approximately orthogonal to the front. Normally, we might expect the front to be quite distinct at this orientation. However, the low level winds ahead of the front are almost directly from the south and are nearly orthogonal to this RHI direction. Therefore, there is virtually no contribution by the wind to the measured Doppler velocities. This tends to reduce the contrast in Doppler velocities across the front. The third RHI ( $226^\circ$ ), to the southwest, shows even less distinction between the velocities in front of and behind the front and there is no vertical continuity to the weak low-level feature.

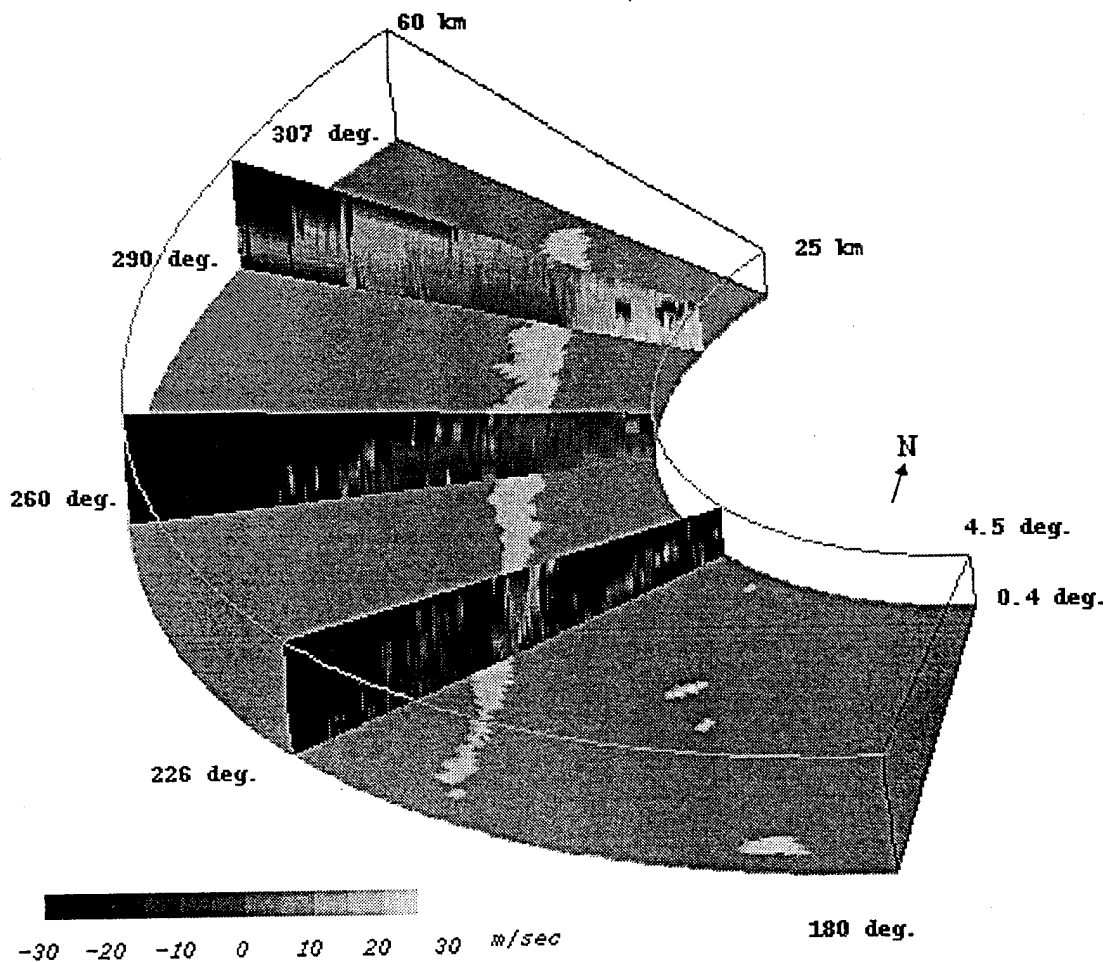


Figure 7. Frontal position as detected at  $0.5^\circ$  elevation and RHI displays of radial velocity at  $226^\circ$ ,  $260^\circ$ , and  $290^\circ$  azimuth.

#### 4.4.2 Reflectivity

Figure 8 shows reflectivity data in RHI planes corresponding to those of Figure 4. Towards the northwest ( $290^\circ$ ), there is a well-defined precipitation core that extends above the surface position of the front and is sheared towards the radar. Some of this slope may be attributable to the significant advection that occurs during the 4 minutes between the lowest and highest scans. However, only about 4 km of this slope can be attributed to advection. On the other hand, the upper level precipitation may reflect convection from further south in the line since the upper level winds are from the south to southwest. These winds would tend to advect the upper portions of the precipitation in a like direction. Towards the west ( $260^\circ$ ), even though the



precipitation is not as strong, there is still a tilt in the upper portions toward the radar. There is still a distinctive line at the lowest level but there is much less vertical structure. It would appear that the convection along the southern portion of the front is less intense than further north.

#### 4.4.3 Gradients

As noted before, the two-dimensional gradients computed at constant elevation (Figure 6) clearly identify frontal position. Figure 9 shows the vertical profiles of radial velocity gradients in RHIs corresponding to those seen in Figures 7 and 8. Again, as in the other two fields, the northernmost plane exhibits the most distinctive structure. The zone of maximum gradients (the dark zone) is somewhat sloped to the right. This is counter to expectations since one would expect fronts to be sloped towards the cold air. However, most, if not all, of this slope can be explained in terms of advection since the front is moving about 15 m/s and the time difference

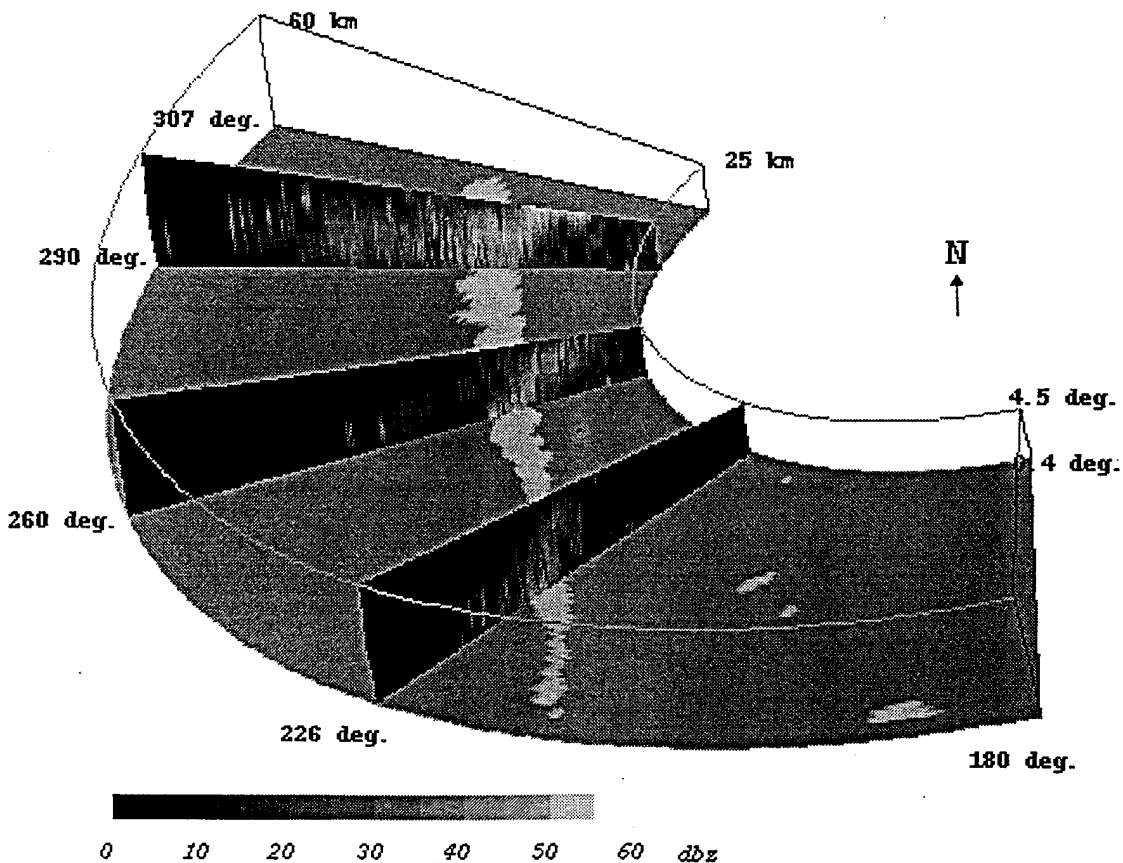


Figure 8. RHI displays of reflectivity as in Figure 7.

from top to bottom for these data is about 4 minutes, thereby resulting in a displacement towards the east of 3.6 km. This would suggest a somewhat vertical front throughout the depth of the observations. The plane towards the west shows somewhat less structure, again consistent with observations in Figures 7 and 8. The southernmost plane shows the least structure.

#### 4.5 SUMMARY

It would appear that the radial velocity fields may contain useful information regarding the intensity of fronts. Locations along the front that have the strongest radial velocity gradients also have the best vertical continuity in all fields and the most intense precipitation activity. Of course, there is somewhat of a chicken and egg problem here that we cannot address with one radar volume. It is not known whether the enhanced precipitation is primarily a result of encountering a region of

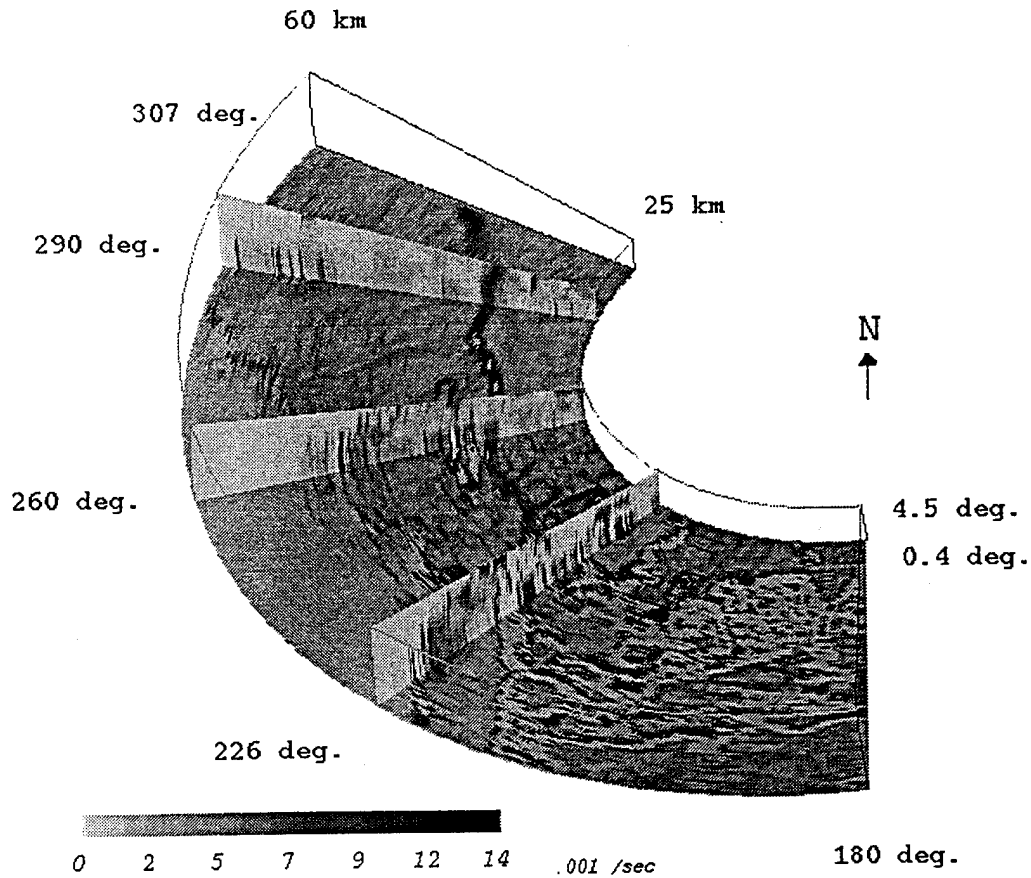


Figure 9. As in Figure 8 but for velocity gradients

more unstable air or to enhanced convergence associated with the front. Also, we do not know why the gradients are enhanced. They could be re-enforced due to downdrafts from the enhanced convective activity. A closer examination of the effects of aspect angle upon gradient computations is required. These are topics for further study.

## **5. DEVIATIONS FROM RESEARCH PLAN**

To date, research on this contract has not progressed as quickly as expected. The original research plan assumed that the government would be acquiring new workstations within the first year of this contract. However, the procurement process proved to be extremely ponderous and the workstations did not arrive until the 18th month. This has impeded progress significantly because initial development was on inadequate computer equipment. The operating systems and software were incompatible with the new systems. After an initial two month learning period for the new Hewlett Packard workstations and AVS software, progress has been greatly accelerated.

## **6. PLANS FOR NEXT CONTRACT YEAR**

During the final year of this contract, HSTX will complete all three tasks as proposed. An algorithm for the monitoring of weak echo regions with time for severe weather prediction will be completed and tested. Another algorithm for the monitoring of the structure of frontal structure will be completed and tested. The utility of storm structure monitoring as a lightning detection tool will be assessed. In all cases a variety of appropriate meteorological events will be used in the testing/assessments.

## **7. REFERENCES**

Branick, M., 1992: NOAA/EFF internal damage survey memo.

Browning, K. A. and R. J. Donaldson, Jr., 1963: Airflow and structure of a tornadic storm. *J. Atmos. Sci.*, **20**, 533-545.

- Browning, K.A. and T.W. Harrold, 1970: Air motion and precipitation growth at a cold front. *QJRMS*, 96, 369-389.
- Chisholm, A. J., 1973: Alberta hailstorms Part 1: Radar case studies and airflow models. *Meteor. Monogr.*, **14**, Amer. Met. Soc., Boston, 1-36.
- Delanoy, R. L. and S. W. Troxel, 1993: Machine intelligent gust front detection. *Linc. Lab. J.*, **6**, 187-212.
- Hamann, 1991: Extraction of fronts from Doppler radar images. Preprints, 25th Conf. on Radar Meteorol., AMS, Boston, MA, pp 119-122.
- Harris, F. I., R. J. Donaldson, Jr., D. J. Smalley, and S. Tung, 1994: Radar studies of aviation hazards: Scientific report No. 1. Phillips Laboratory, PL-TR-94-2146, 84 pp, ADA285845.
- Hobbs, P.V., 1978: Organization and structure of clouds and precipitation on mesoscale and microscale in cyclonic storms. *Rev. Geophys. Space Phys.*, 16, 741-755.
- Klazura, G. E. and D. A. Imy, 1993: A description of the initial set of analysis products available from the NEXRAD WSR-88D system. *Bull. Amer. Met. Soc.*, **74**, 1293-1311.
- Wilson, J.W., and W.E. Schreiber, 1986: Initiation of convective storms at radar observed boundary layer convergence lines. *MWR* 114, 2516-2536.